iScience

CellPress
OPEN ACCESS

Article

Tryptophan Metabolism Regulates Proliferative Capacity of Human Pluripotent Stem Cells

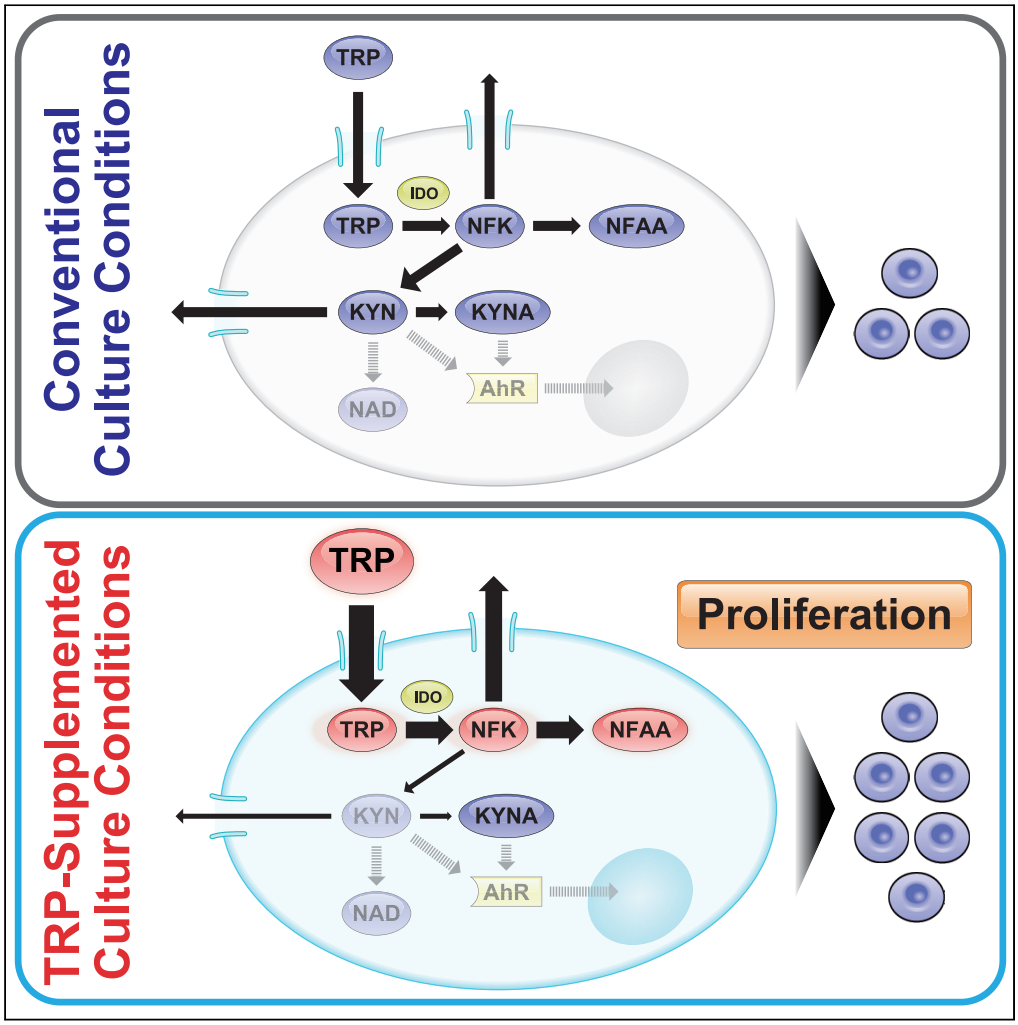

Shota Someya, Shugo Tohyama, Kotaro Kameda, ..., Eiji Kobayashi, Jun Fujita, Keiichi Fukuda

shugotohyama@keio.jp (S.T.)
jfujita@keio.jp (J.F.)

HIGHLIGHTS

TRP is the only AA that enables enhanced hPSC proliferation by supplementation

hPSCs proliferate with pluripotency after long-term culture in TRP supplementation

The proliferative properties of hPSCs are independent of AhR signaling

TRP-derived NFK contributes to enhanced hPSC proliferation

Someya et al., iScience 24, 102090
February 19, 2021
https://doi.org/10.1016/j.isci.2021.102090

iScience

CellPress
OPEN ACCESS

Article

Tryptophan Metabolism Regulates Proliferative Capacity of Human Pluripotent Stem Cells

Shota Someya,[1] Shugo Tohyama,[1,2,5,*] Kotaro Kameda,[1] Sho Tanosaki,[1] Yuika Morita,[1] Kazunori Sasaki,[4] Moon-Il Kang,[4] Yoshikazu Kishino,[1] Marina Okada,[1] Hidenori Tani,[1] Yusuke Soma,[1] Kazuaki Nakajima,[1] Tomohiko Umei,[1] Otoya Sekine,[1] Taijun Moriwaki,[1] Hideaki Kanazawa,[1] Eiji Kobayashi,[2] Jun Fujita,[1,3,*] and Keiichi Fukuda[1]

SUMMARY

Human pluripotent stem cells (hPSCs) have a unique metabolic signature for maintenance of pluripotency, self-renewal, and survival. Although hPSCs could be potentially used in regenerative medicine, the prohibitive cost associated with large-scale cell culture presents a major barrier to the clinical application of hPSC. Moreover, without a fully characterized metabolic signature, hPSC culture conditions are not optimized. Here, we performed detailed amino acid profiling and found that tryptophan (TRP) plays a key role in the proliferation with maintenance of pluripotency. In addition, metabolome analyses revealed that intra- and extracellular kynurenine (KYN) is decreased under TRP-supplemented conditions, whereas N-formylkynurenine (NFK), the upstream metabolite of KYN, is increased thereby contributing to proliferation promotion. Taken together, we demonstrate that TRP is indispensable for survival and proliferation of hPSCs. A deeper understanding of TRP metabolism will enable cost-effective large-scale production of hPSCs, leading to advances in regenerative medicine.

INTRODUCTION

Human pluripotent stem cells (hPSCs), including human embryonic stem cells (hESCs) and human induced pluripotent stem cells (hiPSCs), have the capacity to differentiate into various cell types, making them a promising cell source for regenerative therapy and drug discovery. For clinical applications and industrialization, a large number of cells are needed, which requires large amounts of expensive culture media. To cost-effectively mass-produce cells, hPSCs should be cultured under optimal culture conditions that promote proliferation while maintaining pluripotency.

Metabolism plays a key role in the maintenance of pluripotency and cell survival of hPSCs (Carey et al., 2015; Folmes et al., 2011; Marsboom et al., 2016; Moussaieff et al., 2015; Shiraki et al., 2014; Teslaa et al., 2016; Tohyama et al, 2013, 2016; Vardhana et al., 2019; Wang et al., 2009). hPSCs depend on activated glycolysis and glutamine metabolism for production of ATP, as well as biomass for maintenance of pluripotency and cell survival. Methionine metabolism is also important, because methionine-derived S-adenosylmethionine is a key metabolite for maintaining pluripotency. Understanding the unique metabolism of hPSCs could lead to development of a method for efficient differentiation and elimination of residual undifferentiated stem cells (Marsboom et al., 2016; Shiraki et al., 2014; Tanosaki et al., 2020; Tohyama et al., 2013, 2016; Yanes et al., 2010). However, little is known about optimal concentrations for each amino acid (AA) and the relationship between AA metabolism and proliferation in hPSCs.

We evaluated the consumption profiles and ability of each AA to promote proliferation of hPSCs, focusing on tryptophan (TRP) metabolism. TRP is an essential AA necessary for the integration of protein synthesis. In addition to the production of key metabolites such as serotonin, melatonin, or vitamin B3, it is well known as an important precursor of kynurenine (KYN) and nicotinamide adenine dinucleotide (NAD) stemming from the KYN pathway. The TRP degradation pathway plays an influential role in cancer biology via indoleamine 2,3-dioxygenase (IDO), where KYN acts as a ligand for an aryl hydrocarbon receptor (AhR) to

[1]Department of Cardiology, Keio University School of Medicine, Shinjuku, Tokyo 160-8582, Japan

[2]Department of Organ Fabrication, Keio University School of Medicine, Shinjuku, Tokyo 160-8582, Japan

[3]Endowed Course for Severe Heart Failure Treatment II, Keio University School of Medicine, Shinjuku, Tokyo 160-8582, Japan

[4]Human Metabolome Technologies, Inc., Tsuruoka, Yamagata 997-0052, Japan

[5]Lead Contact

*Correspondence: shugotohyama@keio.jp (S.T.), jfujita@keio.jp (J.F.)

https://doi.org/10.1016/j.isci.2021.102090

promote tumor progression and metastasis (Opitz et al., 2011). An end product of the KYN pathway, NAD, is known to reduce tumorigenesis by minimizing oncogene-induced DNA damage and subsequent carcinogenesis (Tummala et al., 2014). In hPSCs, although it is known that KYN production is greater for the primed state of hPSCs when compared with the naive state (Sperber et al., 2015), and that *AhR* is minimally expressed in hESCs (Cheng et al., 2015), the functionality of the KYN pathway in hPSCs has yet to be fully elucidated.

Here, we show that TRP metabolism plays a key role in promoting proliferation of hPSCs, without the loss of pluripotency. By utilizing this property, we were able to efficiently obtain a large number of hPSCs under TRP-supplemented culture medium conditions, a technique that could lead to clinical applications and industrialization for hPSCs.

RESULTS

TRP supplementation promotes proliferative capacity in hiPSCs

Consumption of AAs in hiPSCs in mTeSR1 maintenance medium over 3 days was first measured by liquid chromatography-tandem mass spectrometry (LC-MS/MS). Consistent with a previous report where AA consumption profiles were evaluated in hESCs under high-glucose DMEM (Tohyama et al., 2016), arginine, cystine, glutamine, and serine were highly consumed. Although aspartate is known to play a key role in the proliferation of cancer cells (Sullivan et al., 2015), no consumption was observed. A previous study has shown that isoleucine, leucine, and methionine are also highly consumed (Shiraki et al., 2014). Interestingly, among all AAs tested in our study, TRP was the most consumed (Figure 1A). We then tested whether AAs have a proliferative effect on hiPSC growth by adding AAs in increments up to 8-fold of the original concentration. We found that TRP was the only AA that caused significant cell growth 5 days post-exposure, in contrast to other AAs such as arginine and lysine, where cell growth was reduced significantly (Figure 1B). Imaging with IncuCyte (Essen BioScience) showed consistent results, and confluence was robustly increased after exposure to incremented TRP concentrations (Figures 1C and S1A).

hPSCs continue to proliferate and maintain pluripotency after long-term culture under TRP-supplemented medium

Next, we determined the optimal cell growth TRP concentration by determining confluence and cell counts. In multiple hPSC lines consisting of both hiPSCs and hESCs, TRP concentration was increased from 4- to 16-fold, and cell confluence showed a corresponding increase, with the most proliferative cells occurring under treatment with a 16-fold TRP concentration (Figures 2A–2C). This enhanced cell growth was preserved through long-term passage up to 10 weeks, and cumulative cell counts of hiPSCs and hESCs were steadily increased across all cell lines, ranging from an approximately 5- to a 17.5-fold increase (Figures 2D and S2A). Interestingly, unlike in hPSCs, TRP supplementation did not significantly promote proliferation in immortalized cell lines, including HeLa and HEK293T cells (Figures S2B and S2C). The ability to retain pluripotency was assessed by various means, including the following: alkaline phosphatase staining, where cells were exposed to TRP-supplemented medium for 5 days; immunocytochemistry staining for NANOG, OCT4, SSEA4, and TRA-1-60 after at least 20 passages; and flow cytometry analysis for SSEA4 and TRA-1-60 after 15 passages. All these staining methods revealed that long-term culture did not deleteriously affect pluripotency markers (Figures 2E and 2F). The karyotype was normal after 4 weeks of culture with treated medium (Figure 2G). These results confirm that hPSCs can be effectively and safely cultured in TRP-supplemented medium without losing key features.

KYN pathway has a pivotal role in proliferation of hiPSCs independent of AhR signaling

Consistent with previous studies (Shiraki et al., 2014), we found that TRP deprivation halted cell growth and led to cell death, and most hiPSCs were incapable of survival after 2 and 4 days of culture in TRP-depleted custom DMEM and TRP-depleted StemFit maintenance medium, respectively (Figure S3A), confirming that TRP is essential in cell growth of hiPSCs and hESCs. To elucidate the mechanism for enhanced proliferation of hPSCs, we first attempted to determine if the KYN pathway has a pivotal role in hPSC proliferation, which is known to lead to the production of KYN, a major ligand for AhR (Opitz et al., 2011), as well as NAD, an important final metabolite of TRP involved in various biochemical reactions, such as glycolysis and oxidative phosphorylation (Purushotham et al., 2009; Rodgers et al., 2005) (Figure 3A). Western blot and immunocytochemistry analysis revealed that hiPSCs have higher IDO expression compared with human cervical cancer (HeLa) cells (Figures 3B and 3C), or differentiated cells, including hiPSC-derived cardiomyocytes and human dermal fibroblasts (Figure S3B). These results were verified by an LC-MS/MS analysis, which demonstrated that KYN was secreted after 3 days of normal maintenance culture (Figure 3D). Knockdown

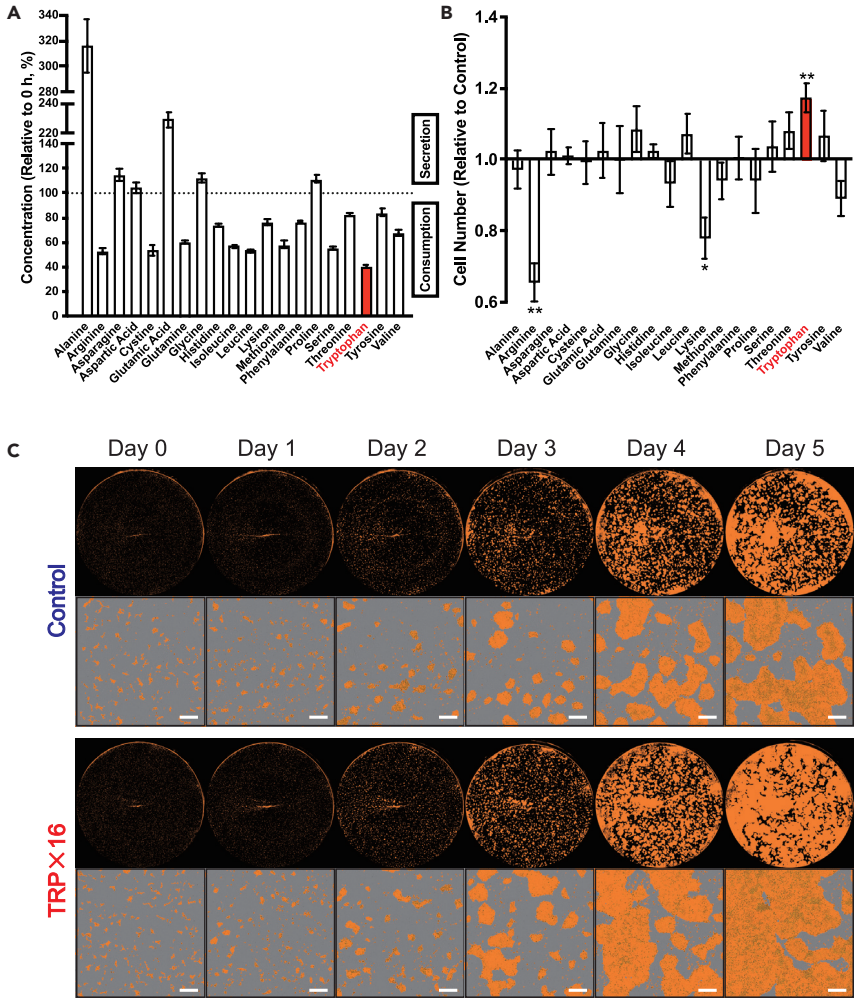

Figure 1. TRP facilitates proliferation of hiPSCs

(A) Consumption of all amino acids (AAs) in hiPSCs (201B7) cultured for 72 h, as determined by liquid chromatography-tandem mass spectrometry (LC-MS/MS) (n = 4 independent experiments).

(B) Cell counts of hiPSCs (201B7) cultured for 7 days. At day 2, the concentration of AAs was increased to 8-fold of the original concentration of mTeSR1. p values were determined by ratio paired t tests comparing the presence or absence of AA augmentation (n = 6 independent experiments; each control value was derived by the average of quadruplicates within the study).

(C) Confluence of hiPSCs (201B7) after 7 days of culture, with 16-fold of the original concentration of tryptophan (TRP) added at 48 h after seeding, versus the control (representative data from n = 6 independent experiments). Scale bar, 500 μm.

Data are represented as mean ± SEM; **p < 0.01.

of *IDO* by small interfering RNA (siRNA) resulted in a reduction of hiPSC cell growth (Figures 3E and 3F), demonstrating that activated IDO is crucial for cell growth of hiPSCs. Next, we tested if abundant expression of AhR plays a role in cell proliferation. In contrast to cancer cell lines, including HeLa, HepG2, and HEK293T cells, AhR expression was scarce in hiPSCs (Figure 3G) and neither its inhibition by siRNA or potent inhibitor StemRegenin-1 (SR-1) influence cell growth capability (Figures 3H, 3I, and S3C) nor did an increase in growth occur with the addition of a potent AhR ligand, 2,3,7,8-tetrachlorodibenzo-p-dioxin (TCDD) (Figure S3D). To analyze the pathway leading to NAD *de novo* synthesis, we first blocked KYN 3-monooxygenase (KMO), a KYN-catalyzing enzyme and important determinant of NAD production, with its potent inhibitor Ro 61-8048, which did not affect cell survival or proliferation (Figure S3E). Addition of a nicotinic acid mononucleotide (a substrate preceding NAD synthesis) did not amplify cell growth (Figure S3F). Furthermore, an NAD/NADH assay using TRP-depleted or TRP-supplemented custom DMEM

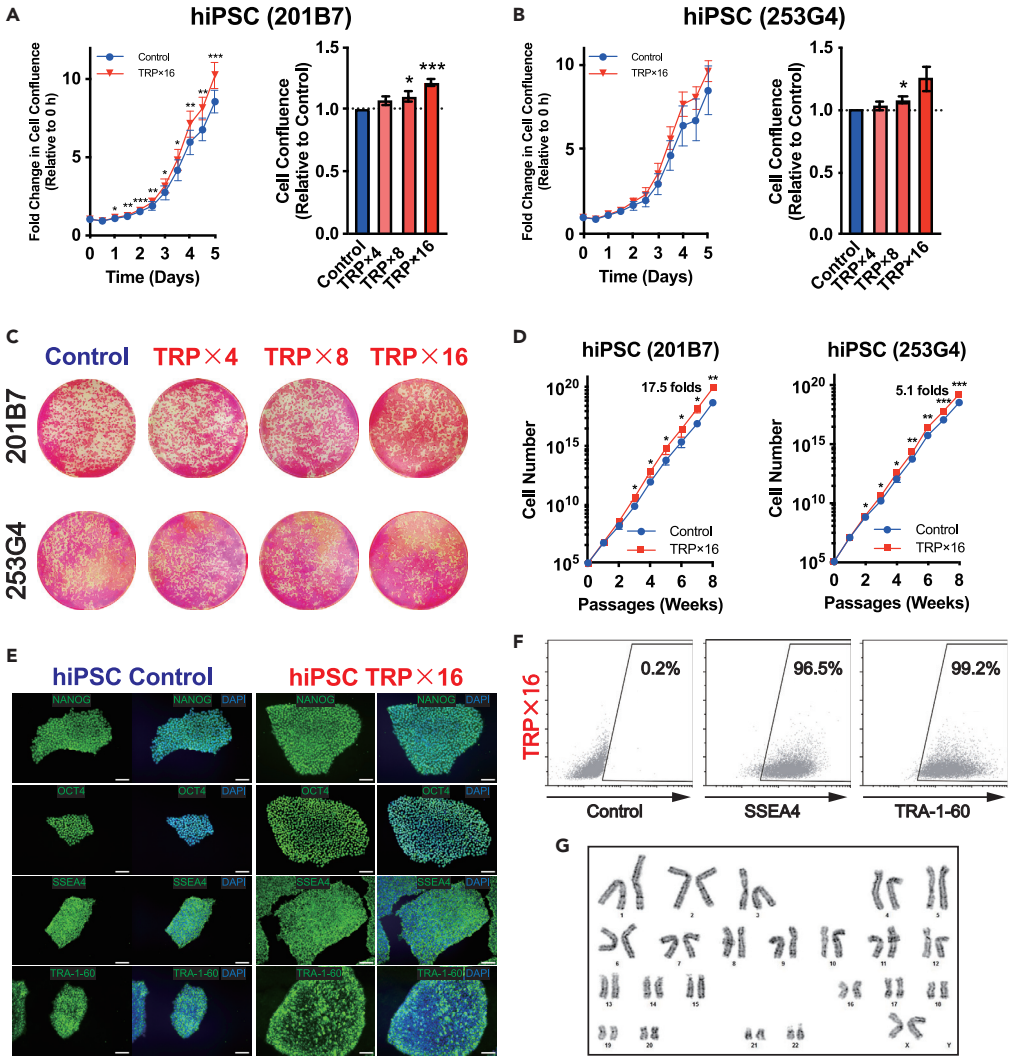

Figure 2. TRP-supplemented medium allows long-term proliferation of hiPSCs with superior efficiency without compromising pluripotency and karyotype

(A and B) Cell confluence after 7 days of hiPSC (201B7 and 253G4) culture, with varying folds of TRP concentration added at 48 h after seeding. p values were determined by ratio paired t test (left) and unpaired t test (right) (n = 6 independent experiments for 201B7; n = 3 independent experiments for 253G4 cell lines).

(C) Alkaline phosphatase staining of hiPSCs (201B7 and 253G4) cultured for 7 days, with different folds of TRP concentrations added at day 2.

(D) Cumulative growth curve of hiPSCs (201B7 and 253G4) cultured in 16-fold TRP-supplemented medium compared with control medium by cell counts. Both cells were adapted to respective medium for at least 1 week before the experiment. p values were determined by ratio paired t test (n = 5 independent experiments).

(E) Immunocytochemistry for NANOG, OCT4, SSEA4, and TRA-1-60, performed on hiPSCs (201B7) after 22 passages of culture with TRP-supplemented medium. Scale bar, 100 μm.

(F) Flow cytometry data indicating SSEA4 and TRA-1-60 levels of hiPSCs (201B7) after maintenance in TRP-supplemented medium for 15 passages (representative data from three independent experiments).

(G) Normal karyotype analysis of hiPSCs (201B7) cultured in 16-fold TRP-supplemented medium for 4 weeks.

Data are represented as mean ± SEM; *p < 0.05; **p < 0.01; ***p < 0.001.

demonstrated that 24 h of TRP depletion or supplementation neither significantly altered the total NAD and NADH nor the NAD/NADH ratio (Figure S3G). Finally, to test the role of aspartate, which is crucial for cancer cell proliferation and for the maintenance of an optimal NAD/NADH ratio (Gui et al., 2016), we supplemented hiPSCs with up to a 10 mM concentration of aspartate, which is above physiological concentrations, and observed no proliferative benefit (Figure S3H).

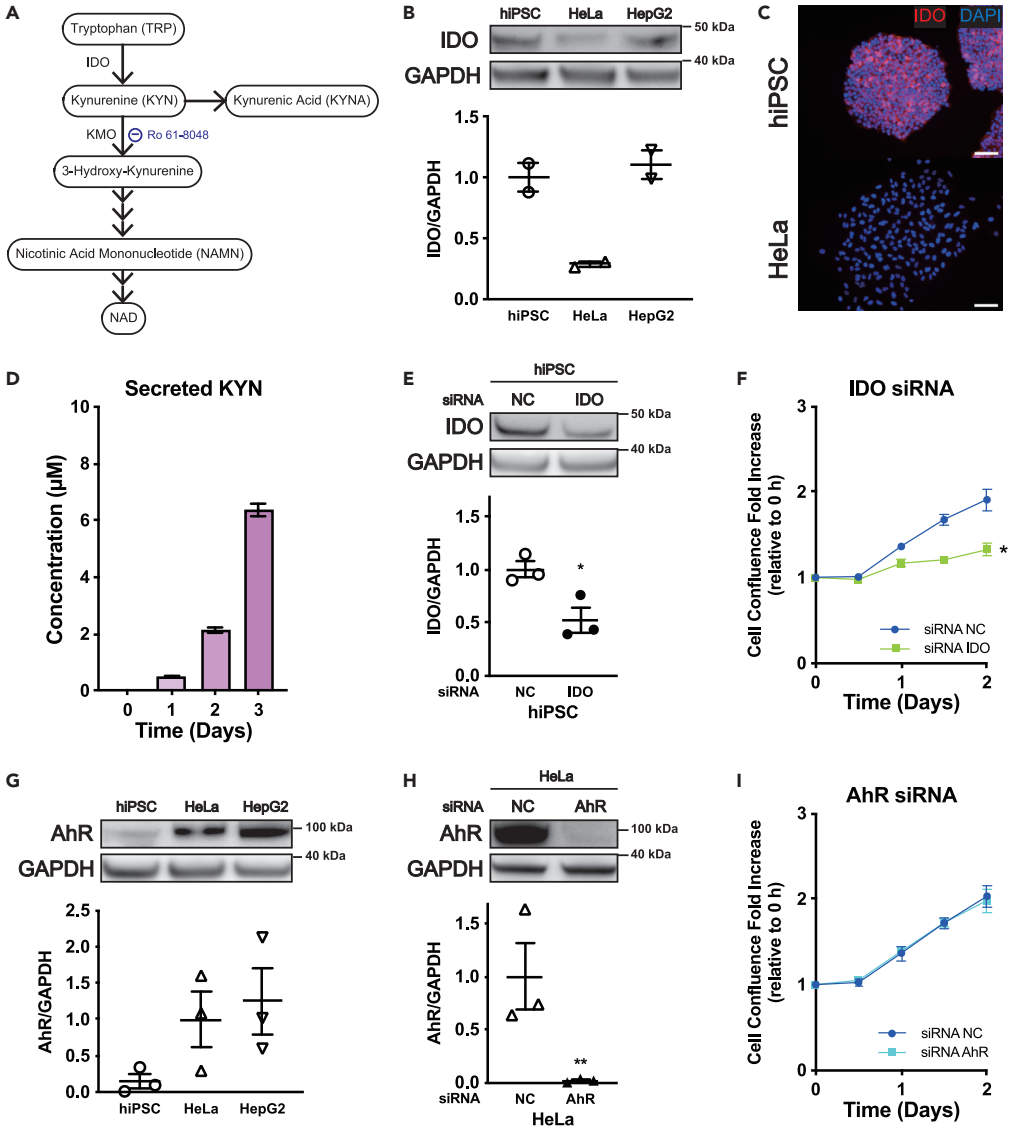

Figure 3. Activation of the KYN pathway via IDO, but not AhR, is crucial for hiPSC survival

(A) TRP pathway leading to nicotinamide adenine dinucleotide (NAD) and kynurenic acid (KYNA). IDO, indoleamine 2,3-dioxygenase; KMO, kynurenine 3-monooxygenase.

(B) Representative immunoblot protein expressions of IDO in hiPSCs (201B7), HeLa, and HepG2 cells by western blot, and the relative quantified protein expressions of IDO, in which hiPSC levels were set to 1. GAPDH was used as a loading control (n = 2).

(C) Immunocytochemistry of IDO in hiPSCs (201B7) and HeLa cells. Scale bar, 100 μm.

(D) Serial concentrations of kynurenine (KYN) secreted in medium cultured for 3 days (n = 4 independent experiments).

(E) Western blot and the relative protein expression of IDO and GAPDH in hiPSCs (201B7) after *IDO* or negative control (NC) siRNA knockdown. Values were normalized to negative controls. p values were determined by a ratio paired t test (n = 3).

(F and I) Proliferation assays of hiPSCs (201B7), performed after seeding 2.5 × 10^5 cells and 24 h of culture under normal conditions followed by 48-h lipofection with *IDO* or *AhR* (aryl hydrocarbon receptor) siRNA knockdown, comparing against NC siRNA. p values were determined with an unpaired t test (n = 3 independent experiments).

(G) AhR levels by western blot and their relative protein expressions were normalized to those of HeLa cells (n = 3).

(H) Western blot analysis and the relative protein expressions of AhR and GAPDH in HeLa cells after NC or *AhR* siRNA knockdown. Values were normalized to negative controls. p values were determined with a ratio paired t test (n = 3).

Data are represented as mean ± SEM; *p < 0.05; **p < 0.01.

KYN is decreased and NFK is increased under TRP-supplemented conditions

We initially attempted to quantify metabolites of the KYN pathway by utilizing conventional metabolome analysis, by employing capillary electrophoresis time-of-flight mass spectrometry (CE-TOFMS). One drawback of this method is that we could not detect key intermediate metabolites apart from KYN, NAD, and NADH (**data not shown**). In comparison, by applying our newly developed capillary electrophoresis coupled with a Fourier transform mass spectrometry (CE-FTMS) platform to evaluate metabolomics data (Sasaki et al., 2019), we successfully detected a wider range of metabolites, including those of the KYN pathway. We performed a metabolome analysis using CE-FTMS to determine how TRP-supplemented medium influences metabolomics profiles of hiPSCs and compared the metabolites after 24- and 48-h exposure to treated medium. With the exception of isocitrate, metabolites relevant to glycolysis and the tricarboxylic acid cycle did not differ significantly between the conventional and TRP-supplemented media groups at 24 h (Figure S4A). To further determine if glycolysis or oxidative phosphorylation is affected upon TRP metabolism, the flux analyzer was used, which demonstrated no differences in extracellular acidification rate and oxidative consumption rate between the two groups (Figures S4B and S4C). Moreover, hiPSCs contained large amounts of intracellular TRP, following exposure to treated medium (Figures S4D and S4E), with the first-step metabolite, N-formylkynurenine (NFK), increased by up to 3-fold after 24- and 48-h exposure (Figures 4A, 4B, and S4F). Meanwhile, although NFK-derived N-formylanthranilic acid (NFAA) was transiently increased at 24 h, no significant difference was observed at 48 h. Furthermore, KYN demonstrated a general decreased trend ($P = 0.0672$ at 24 h), whereas the concentration of metabolite quinolinic acid, as well as those of both NAD and NADH, were unchanged up to 24 h. These results agree with those observed in the NAD/NADH assay, despite an unexpected decrease in NAD observed at 48 h (Figures S3G and S4F). The change in flux of TRP metabolites observed by CE-FTMS was consistent with the results obtained from a conventional LC-MS/MS analysis, which demonstrated that whereas secretions of TRP and NFK were consistently elevated, KYN was significantly decreased following TRP supplementation (Figures 4C–4E). An additional metabolome analysis was performed to describe the flux in TRP metabolism by comparing TRP-depleted and TRP-replenished media. Results show that the 6-h depletion leads to significant decreases in TRP, NFK, and KYN, demonstrating that TRP is indispensable in maintaining downstream metabolites of the KYN pathway (Figure S4G). Next, to identify the TRP metabolite responsible for promoting hiPSC proliferation, we assessed the cell proliferation capacity following addition of NFK, which manifested a significant increase in cell confluence (Figure 4F). Taken together, these results imply that TRP, the most consumed AA in hiPSCs, contributes to proliferation when supplemented medium is used, yet this contribution is independent of the catabolism of TRP into KYN and NAD, but rather by increasing the concentration of NFK, thereby bypassing the stimulation of minimally expressed AhR, or upregulation of glycolysis and oxidative phosphorylation by NAD (Figure 4G).

DISCUSSION

In this study, we evaluated detailed AA profiling in hPSCs and found that TRP was indispensable for survival and proliferation of hPSCs. Consistent with previous studies, arginine, cystine, glutamine, methionine, serine, and TRP were highly consumed AAs, regardless of cell line or culture medium (Tohyama et al., 2016). Recently, some reports have shown that most of these AAs play key roles in the maintenance of pluripotency and survival (Marsboom et al., 2016; Shiraki et al., 2014). However, few studies have examined the role of TRP in hPSC culture maintenance. We demonstrated that TRP supplementation significantly increased proliferative capacity of hPSCs, suggesting that the concentration of TRP in conventional hPSC maintenance media is suboptimal for inducing efficient proliferation. In contrast, supplementation with the other AAs did not promote proliferation, suggesting that concentrations of these AAs are already optimal.

The metabolic signature of hPSCs resembles that of cancer cells in some aspects, as both cells strongly rely on aerobic glycolysis and glutamine oxidation as sources of energy expenditure and biomass production. TRP was shown to be highly consumed in hiPSCs, which was similar to previous findings in cancer cells (Opitz et al., 2011; Snodgrass and Iversen, 1974). Interestingly, TRP supplementation did not directly promote proliferation in cancer cells, whereas it significantly promoted proliferation in hPSCs. In cancer cells, a main purpose of TRP metabolism through IDO is to produce KYN for suppression of antitumor immune T cells via AhR signaling, thus creating a suitable tumor microenvironment that indirectly leads to increased growth (Opitz et al., 2011). Clinically, the level of IDO expressions is known to positively correlate with poor prognosis in some cancers, thus prompting the use of IDO inhibitors, some of which are undergoing clinical trials for cancer chemotherapy (Prendergast et al., 2017). In hiPSCs, IDO was richly expressed, and its

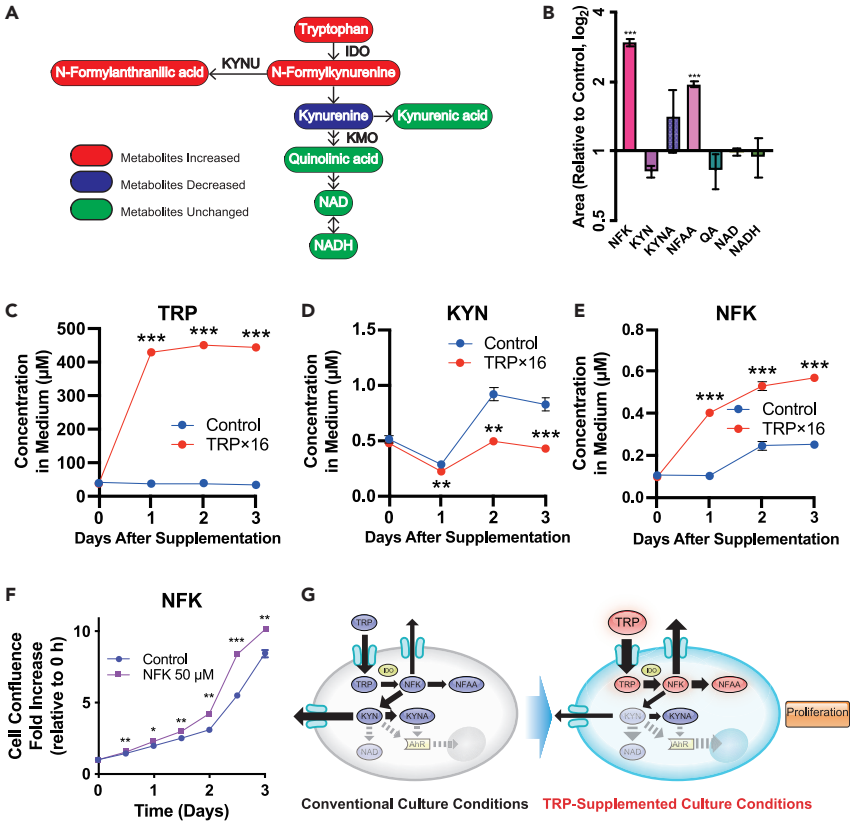

Figure 4. Metabolomic analysis of the TRP pathway in hiPSCs

(A) TRP pathway comparing hiPSCs (201B7) incubated with or without TRP-supplemented medium for 24 h, as analyzed by CE-FTMS, where the red or blue coloring indicates increased or decreased metabolites, respectively, and green denotes metabolites that are unchanged (n = 5 replicates).

(B) Change in the normalized relative intracellular concentrations of KYN pathway metabolites after TRP exposure for 24 h as determined by CE-FTMS. p values were determined with an unpaired t test, comparing the raw results of each metabolite (n = 5 replicates). NFK, N-formylkynurenine; NFAA, N-formylanthranilic acid; QA, quinolinic acid; others are as mentioned previously.

(C–E) Serial extracellular concentrations of TRP, KYN, and NFK, respectively, with or without TRP-supplemented medium for 3 days, analyzed by LC-MS/MS. p values were determined by an unpaired t test (n = 4 replicates).

(F) Cell confluence after 5 days of hiPSC (201B7) culture in StemFit maintenance medium, with NFK added at 48 h after seeding. p values were determined by unpaired t test (n = 3).

(G) Synoptic diagram indicating the influx of TRP and catabolism of KYN pathway metabolites in hiPSCs, with or without supplementation of TRP-supplemented medium, highlighting diminished change in flux of metabolites distal to NFK.

Data are represented as mean ± SEM; $p < 0.05$; $p < 0.01$; $p < 0.001$.

inhibition by siRNA knockdown resulted in termination of cell growth, confirming that TRP catabolism is vital for survival of hiPSCs. In contrast, whether AhR signaling is directly associated with cancer cell proliferation remains unclear; nevertheless, it seems to affect proliferative capacity in some cancer cells. For instance, *AhR* knockdown in HepG2 cells was shown to decrease cell proliferation due to downregulation of cell-cycle-related genes (Abdelrahim et al., 2003), whereas agonism of AhR by TCDD was shown to suppress cell proliferation of OVCAR-3, a human ovarian cancer cell line (Li et al., 2014). It was also reported that TRP derivatives negatively regulate cancer cell stemness via AhR signaling, reducing tumorigenicity (Cheng et al., 2015). Aside from cancer cells, immune B cells require functional AhR to optimally proliferate, through activation of cyclin O (Villa et al., 2017). In contrast to cancer cells, we demonstrated that AhR was negligibly expressed in hiPSCs, and its inhibition did not affect cell survival and proliferation, highlighting a distinct signaling property of hPSCs.

To quantify intracellular metabolites under TRP-supplemented conditions or TRP-depleted conditions, we performed CE-FTMS-based metabolome analysis. Conventional CE-TOFMS is a powerful tool to detect

both intracellular and extracellular metabolites. However, detection of small amounts of metabolites in the KYN pathway was challenging. To solve this problem, we applied CE-FTMS (Sasaki et al., 2019; Soga and Heiger, 2000; Soga et al, 2002, 2003). Our CE-FTMS-based metabolome analysis showed that supplementation with TRP did not significantly increase the concentration of KYN and kynurenic acid (KYNA), which may also act as an AhR agonist, but significantly increased NFK and NFAA, suggesting that upstream metabolites of KYN contribute to promoting proliferation in hPSCs. These findings support those demonstrating that NFK, rather than its downstream metabolites, are involved in promoting proliferation of hiPSCs.

TRP metabolism also contributes to NAD *de novo* synthesis, which regulates proliferation and metabolism in cancer cells (Tummala et al., 2014). In addition, the presence of NAD is known to be crucial for survival of hiPSCs (Son et al., 2013). However, our study revealed that TRP supplementation did not affect NAD production via the KYN pathway, and TRP deprivation alone did not affect either NAD/NADH ratio or NAD concentration, possibly indicating that NAD production from the salvage pathway or elsewhere is more important than the *de novo* pathway. Thus, TRP-derived NAD does not contribute to promoting survival and proliferation in hPSCs.

Multiple clinical trials in regenerative medicine with hPSCs are currently ongoing. However, the risk of tumorigenicity, as well as prohibitive costs associated with large-scale cell culture, are major barriers to hPSC use in the clinic and industrialization. To address risk of tumorigenicity, we previously developed an innovative method to eliminate undifferentiated stem cells and achieve purification of differentiated cells by altering culture conditions, based on an understanding of metabolic signature in hPSCs (Shiraki et al., 2014; Tanosaki et al., 2020; Tohyama et al., 2013, 2016; Wang et al., 2009). The results of this study suggest that regulation of TRP metabolism promotes proliferative capacity in hPSCs, indicating that large numbers of hPSCs can efficiently be produced at a low cost by improving culture conditions. Understanding unique metabolic signatures of hPSCs will enable advances in regenerative medicine and drug discovery.

Limitations of the study

Despite the observation that TRP and its downstream metabolite NFK cause increased cell proliferation, the underlying molecular and signaling events regulating cell growth remain to be elucidated, and further study is warranted to strengthen our understanding of a metabolic signature of hPSCs.

Resources availability

Lead contact

Further information and requests for resources and reagents should be directed to and will be fulfilled by the Lead Contact, Shugo Tohyama, Keio University (shugotohyama@keio.jp).

Materials availability

This study did not generate new unique reagents.

Data and code availability

There is no dataset and/or code associated with the article.

METHODS

All methods can be found in the accompanying Transparent Methods supplemental file.

SUPPLEMENTAL INFORMATION

Supplemental information can be found online at https://doi.org/10.1016/j.isci.2021.102090.

ACKNOWLEDGMENTS

The authors thank Drs. Satoru Okamoto and Kotoe Koseki for analysis of amino acids consumption profiles in culture media (Ajinomoto); Tomoko Haruna, Rei Ohno, Sayaka Kanaami, Chihana Fujita, Miho Yamaguchi, Yui Narita, and Naoko Matsumoto for technical assistance with cell preparation and culture (Department of Cardiology, Keio University); Dr. Erina Sugita for technical assistance with Extracellular Flux

Analyzer (Department of Endocrinology, Metabolism and Nephrology, Keio University); and Dr. Kenichiro Kinouchi for fruitful discussions (Department of Endocrinology, Metabolism and Nephrology, Keio University). The authors also thank the Center for iPSC Research and Application, and Kyoto University, for the 253G4 and 201B7 cell lines, and WiCell research institute for H9 ES cells. The present work was mainly supported by Projects for Technological Development, Research Center Network for Realization of Regenerative Medicine by Japan, the Japan Agency for Medical Research and Development (AMED) grant 20bm0404023h0003 to S. Tohyama, and partly supported by the Highway Program for Realization of Regenerative Medicine from AMED grant 19bk0104062h0003 to K.F., HMT Research Grant for Young Leaders in Metabolomics to S. Tohyama, and the Japan Society for the Promotion of Science (JSPS) KAKENHI 19K22626 to S. Tohyama.

AUTHOR CONTRIBUTION

S. Tohyama and J.F. conceptualized the study; S. Tohyama designed the study; S.S. performed and analyzed most experiments; K.K., S.Tanosaki, Y.M., K.S., M.-I.K., Y.K., M.O., H.T., Y.S., K.N., T.U., O.S., T.M., and H.K. contributed to specific experiments; S. Tohyama and S.S. wrote the original draft; S. Tohyama, J.F., and K.F. wrote, reviewed, and edited the manuscript; S. Tohyama and K.F acquired funding; S. Tohyama, J.F., and K.F. supervised the study.

DECLARATION OF INTERESTS

S.S., S. Tohyama, J.F., and K.F. have a patent pending related to this work. K.F. is a co-founder and CEO of Heartseed, Inc. S. Tohyama is an advisor of Heartseed, Inc. S. Tohyama, J.F., H.K., and K.F. own equity in Heartseed, Inc. The remaining authors have no conflicts of interest to disclose.

Received: November 2, 2020
Revised: November 9, 2020
Accepted: January 18, 2021
Published: February 19, 2021

REFERENCES

Abdelrahim, M., Smith, R., and Safe, S. (2003). Aryl hydrocarbon receptor gene silencing with small inhibitory RNA differentially modulates Ah-responsiveness in MCF-7 and HepG2 cancer cells. Mol. Pharmacol. *63*, 1373–1381.

Carey, B.W., Finley, L.W.S., Cross, J.R., Allis, C.D., and Thompson, C.B. (2015). Intracellular α-ketoglutarate maintains the pluripotency of embryonic stem cells. Nature *518*, 413–416.

Cheng, J., Li, W., Kang, B., Zhou, Y., Song, J., Dan, S., Yang, Y., Zhang, X., Li, J., Yin, S., et al. (2015). Tryptophan derivatives regulate the transcription of Oct4 in stem-like cancer cells. Nat. Commun. *6*, 7209.

Folmes, C.D.L., Nelson, T.J., Martinez-Fernandez, A., Arrell, D.K., Lindor, J.Z., Dzeja, P.P., Ikeda, Y., Perez-Terzic, C., and Terzic, A. (2011). Somatic oxidative bioenergetics transitions into pluripotency-dependent glycolysis to facilitate nuclear reprogramming. Cell Metab. *14*, 264–271.

Gui, D.Y., Sullivan, L.B., Luengo, A., Hosios, A.M., Bush, L.N., Gitego, N., Davidson, S.M., Freinkman, E., Thomas, C.J., and Vander Heiden, M.G. (2016). Environment dictates dependence on mitochondrial complex I for NAD+ and aspartate production and determines cancer cell sensitivity to metformin. Cell Metab. *24*, 716–727.

Li, Y., Wang, K., Jiang, Y.-Z., Chang, X.-W., Dai, C.-F., and Zheng, J. (2014). 2,3,7,8-Tetrachlorodibenzo-p-dioxin (TCDD) inhibits human ovarian cancer cell proliferation. Cell Oncol (Dordr) *37*, 429–437.

Marsboom, G., Zhang, G.-F., Pohl-Avila, N., Zhang, Y., Yuan, Y., Kang, H., Hao, B., Brunengraber, H., Malik, A.B., and Rehman, J. (2016). Glutamine metabolism regulates the pluripotency transcription factor OCT4. Cell Rep. *16*, 323–332.

Moussaieff, A., Rouleau, M., Kitsberg, D., Cohen, M., Levy, G., Barasch, D., Nemirovski, A., Shen-Orr, S., Laevsky, I., Amit, M., et al. (2015). Glycolysis-mediated changes in acetyl-CoA and histone acetylation control the early differentiation of embryonic stem cells. Cell Metab. *21*, 392–402.

Opitz, C.A., Litzenburger, U.M., Sahm, F., Ott, M., Tritschler, I., Trump, S., Schumacher, T., Jestaedt, L., Schrenk, D., Weller, M., et al. (2011). An endogenous tumour-promoting ligand of the human aryl hydrocarbon receptor. Nature *478*, 197–203.

Prendergast, G.C., Malachowski, W.P., DuHadaway, J.B., and Muller, A.J. (2017). Discovery of Ido1 inhibitors: from bench to bedside. Cancer Res. *77*, 6795–6811.

Purushotham, A., Schug, T.T., Xu, Q., Surapureddi, S., Guo, X., and Li, X. (2009). Hepatocyte-specific deletion of SIRT1 alters fatty acid metabolism and results in hepatic steatosis and inflammation. Cell Metab. *9*, 327–338.

Rodgers, J.T., Lerin, C., Haas, W., Gygi, S.P., Spiegelman, B.M., and Puigserver, P. (2005). Nutrient control of glucose homeostasis through a complex of PGC-1alpha and SIRT1. Nature *434*, 113–118.

Sasaki, K., Sagawa, H., Suzuki, M., Yamamoto, H., Tomita, M., Soga, T., and Ohashi, Y. (2019). Metabolomics platform with capillary electrophoresis coupled with high-resolution mass spectrometry for plasma analysis. Anal. Chem. *91*, 1295–1301.

Shiraki, N., Shiraki, Y., Tsuyama, T., Obata, F., Miura, M., Nagae, G., Aburatani, H., Kume, K., Endo, F., and Kume, S. (2014). Methionine metabolism regulates maintenance and differentiation of human pluripotent stem cells. Cell Metab. *19*, 780–794.

Snodgrass, S.R., and Iversen, L.L. (1974). Amino acid uptake into human brain tumors. Brain Res. *76*, 95–107.

Soga, T., and Heiger, D.N. (2000). Amino acid analysis by capillary electrophoresis electrospray ionization mass spectrometry. Anal. Chem. *72*, 1236–1241.

Soga, T., Ohashi, Y., Ueno, Y., Naraoka, H., Tomita, M., and Nishioka, T. (2003). Quantitative metabolome analysis using capillary electrophoresis mass spectrometry. J. Proteome Res. *2*, 488–494.

Soga, T., Ueno, Y., Naraoka, H., Ohashi, Y., Tomita, M., and Nishioka, T. (2002). Simultaneous determination of anionic intermediates for Bacillus subtilis metabolic pathways by capillary electrophoresis electrospray ionization mass spectrometry. Anal. Chem. *74*, 2233–2239.

Son, M.J., Son, M.-Y., Seol, B., Kim, M.-J., Yoo, C.H., Han, M.-K., and Cho, Y.S. (2013). Nicotinamide overcomes pluripotency deficits and reprogramming barriers. Stem Cells *31*, 1121–1135.

Sperber, H., Mathieu, J., Wang, Y., Ferreccio, A., Hesson, J., Xu, Z., Fischer, K.A., Devi, A., Detraux, D., Gu, H., et al. (2015). The metabolome regulates the epigenetic landscape during naive-to-primed human embryonic stem cell transition. Nat. Cell Biol. *17*, 1523–1535.

Sullivan, L.B., Gui, D.Y., Hosios, A.M., Bush, L.N., Freinkman, E., and Vander Heiden, M.G. (2015). Supporting aspartate biosynthesis is an essential function of respiration in proliferating cells. Cell *162*, 552–563.

Tanosaki, S., Tohyama, S., Fujita, J., Someya, S., Hishiki, T., Matsuura, T., Nakanishi, H., Ohto-Nakanishi, T., Akiyama, T., Morita, Y., et al. (2020). Fatty acid synthesis is indispensable for survival of human pluripotent stem cells. iScience *23*, 101535.

Teslaa, T., Chaikovsky, A.C., Lipchina, I., Escobar, S.L., Hochedlinger, K., Huang, J., Graeber, T.G., Braas, D., and Teitell, M.A. (2016). α-Ketoglutarate accelerates the initial differentiation of primed human pluripotent stem cells. Cell Metab. *24*, 485–493.

Tohyama, S., Fujita, J., Hishiki, T., Matsuura, T., Hattori, F., Ohno, R., Kanazawa, H., Seki, T., Nakajima, K., Kishino, Y., et al. (2016). Glutamine oxidation is indispensable for survival of human pluripotent stem cells. Cell Metab. *23*, 663–674.

Tohyama, S., Hattori, F., Sano, M., Hishiki, T., Nagahata, Y., Matsuura, T., Hashimoto, H., Suzuki, T., Yamashita, H., Satoh, Y., et al. (2013). Distinct metabolic flow enables large-scale purification of mouse and human pluripotent stem cell-derived cardiomyocytes. Cell Stem Cell *12*, 127–137.

Tummala, K.S., Gomes, A.L., Yilmaz, M., Graña, O., Bakiri, L., Ruppen, I., Ximénez-Embún, P., Sheshappanavar, V., Rodriguez-Justo, M., Pisano, D.G., et al. (2014). Inhibition of de novo NAD(+) synthesis by oncogenic URI causes liver tumorigenesis through DNA damage. Cancer Cell *26*, 826–839.

Vardhana, S.A., Arnold, P.K., Rosen, B.P., Chen, Y., Carey, B.W., Huangfu, D., Carmona-Fontaine, C., Thompson, C.B., and Finley, L.W.S. (2019). Glutamine independence is a selectable feature of pluripotent stem cells. Nat. Metab. *1*, 676–687.

Villa, M., Gialitakis, M., Tolaini, M., Ahlfors, H., Henderson, C.J., Wolf, C.R., Brink, R., and Stockinger, B. (2017). Aryl hydrocarbon receptor is required for optimal B-cell proliferation. Embo J. *36*, 116–128.

Wang, J., Wang, J., Alexander, P., Alexander, P., Wu, L., Wu, L., Hammer, R., Hammer, R., Cleaver, O., Cleaver, O., et al. (2009). Dependence of mouse embryonic stem cells on threonine catabolism. Science *325*, 435–439.

Yanes, O., Clark, J., Wong, D.M., Patti, G.J., Sánchez-Ruiz, A., Benton, H.P., Trauger, S.A., Desponts, C., Ding, S., and Siuzdak, G. (2010). Metabolic oxidation regulates embryonic stem cell differentiation. Nat. Chem. Biol. *6*, 411–417.

iScience, Volume *24*

Supplemental Information

Tryptophan Metabolism Regulates Proliferative Capacity of Human Pluripotent Stem Cells

Shota Someya, Shugo Tohyama, Kotaro Kameda, Sho Tanosaki, Yuika Morita, Kazunori Sasaki, Moon-Il Kang, Yoshikazu Kishino, Marina Okada, Hidenori Tani, Yusuke Soma, Kazuaki Nakajima, Tomohiko Umei, Otoya Sekine, Taijun Moriwaki, Hideaki Kanazawa, Eiji Kobayashi, Jun Fujita, and Keiichi Fukuda

Figure S1

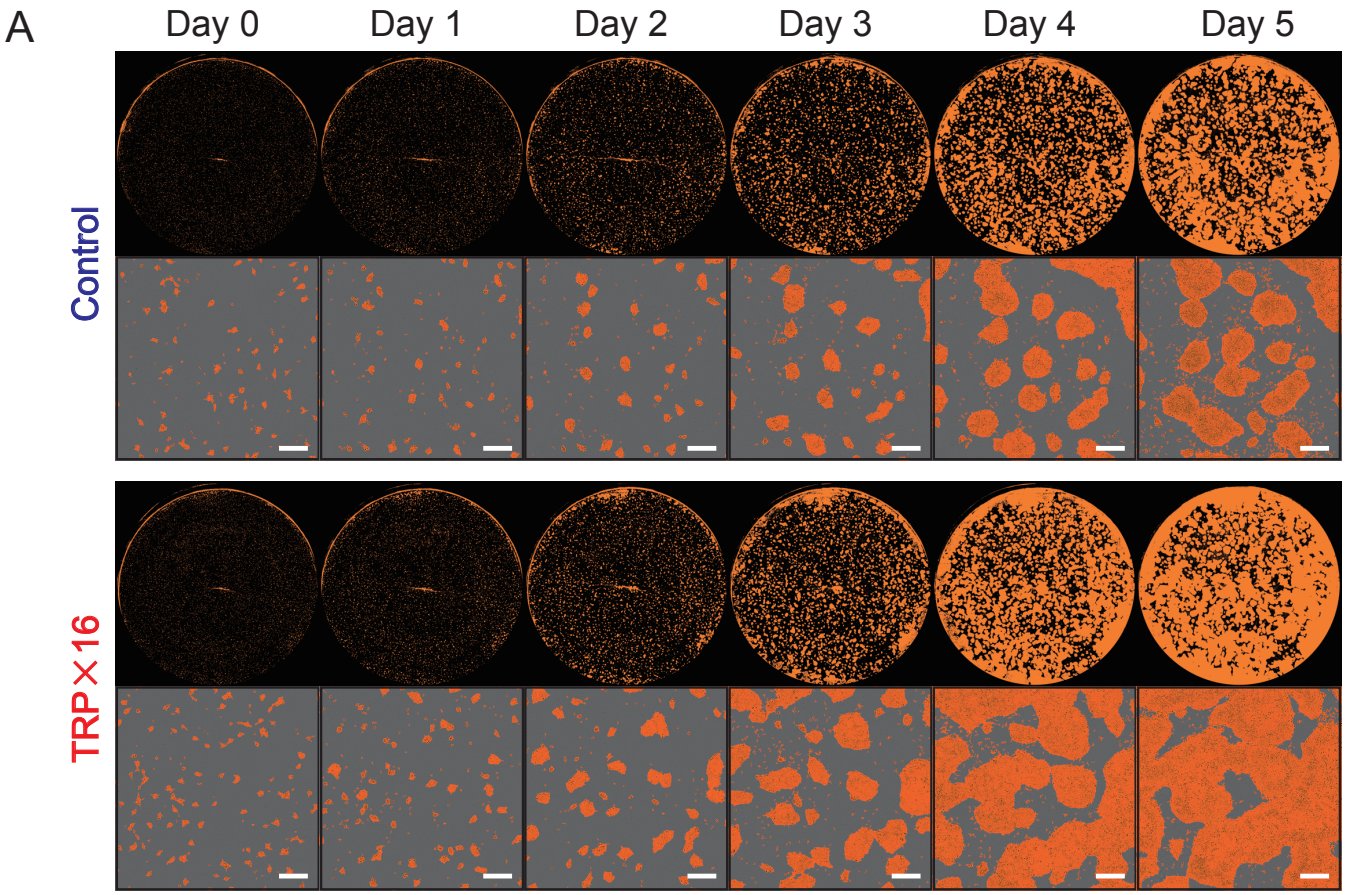

Figure S2

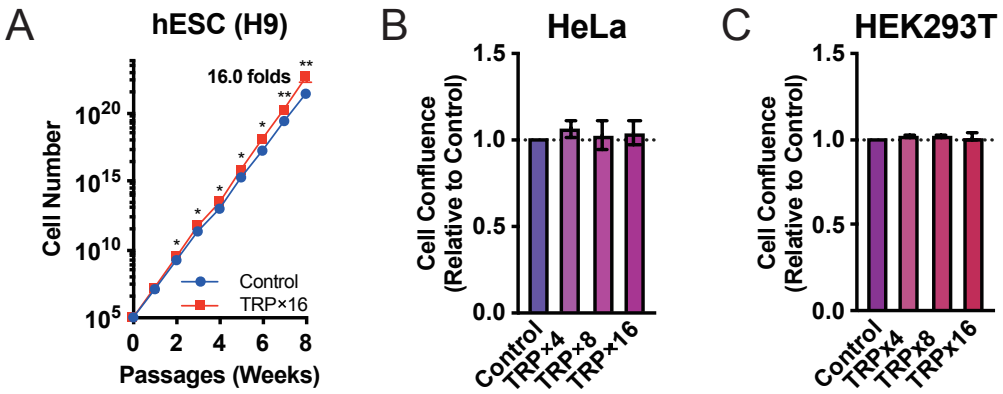
A
hESC (H9)
16.0 folds
Cell Number
10^{20}
10^{15}
10^{10}
10^{5}
Control
TRP×16
0 2 4 6 8
Passages (Weeks)
B
HeLa
Cell Confluence (Relative to Control)
1.5
1.0
0.5
0.0
Control
TRP×4
TRP×8
TRP×16
C
HEK293T
Cell Confluence (Relative to Control)
1.5
1.0
0.5
0.0
Control
TRPx4
TRPx8
TRPx16

Figure S3

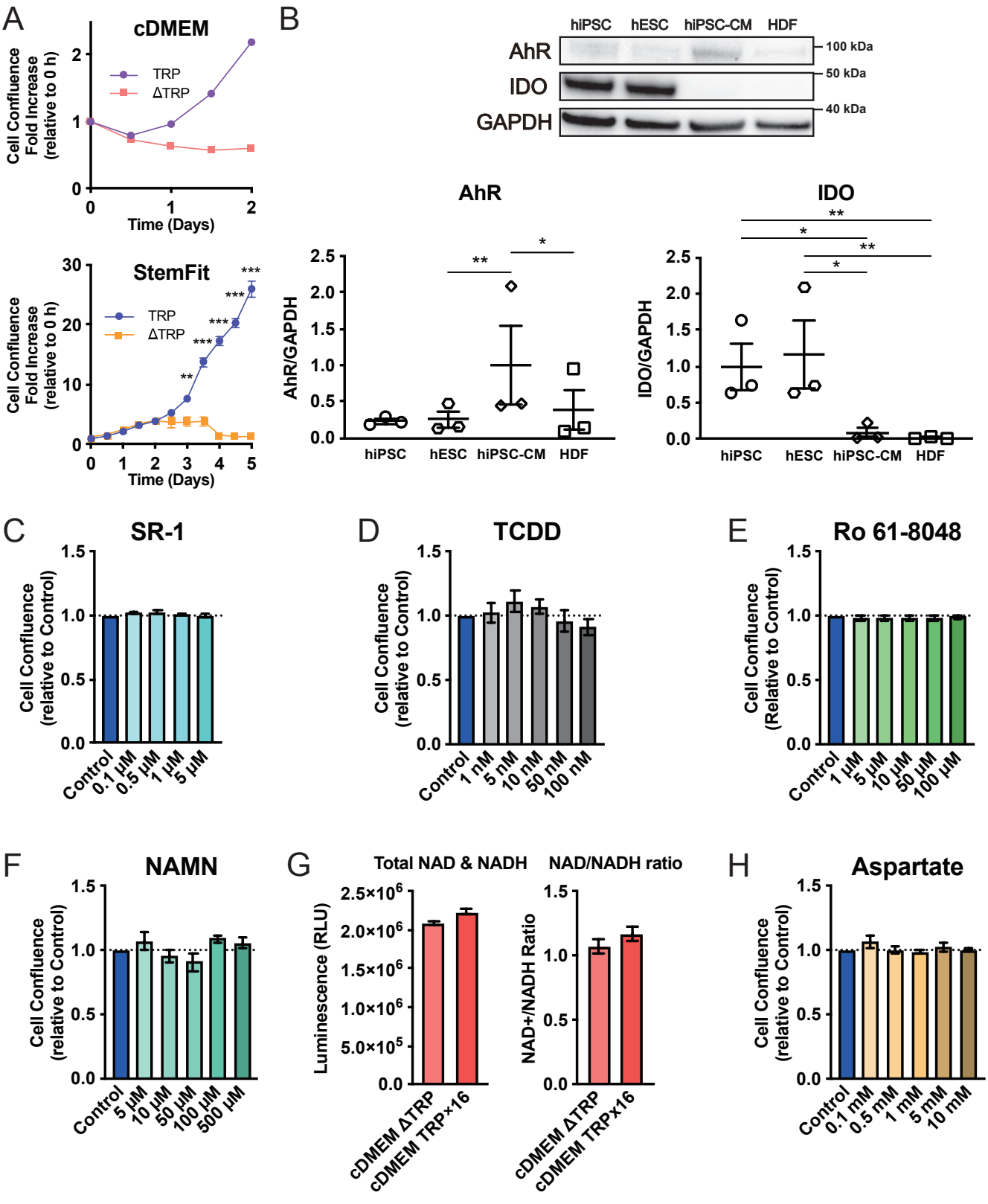
A
cDMEM
Cell Confluence Fold Increase (relative to 0 h)
TRP
ΔTRP
Time (Days)
StemFit
B
hiPSC
hESC
hiPSC-CM
HDF
AhR
IDO
GAPDH
100 kDa
50 kDa
40 kDa
AhR/GAPDH
IDO/GAPDH
C
SR-1
Cell Confluence (relative to Control)
Control
0.1 μM
0.5 μM
1 μM
5 μM
D
TCDD
1 nM
5 nM
10 nM
50 nM
100 nM
E
Ro 61-8048
Cell Confluence (Relative to Control)
1 μM
5 μM
10 μM
50 μM
100 μM
F
NAMN
5 μM
10 μM
50 μM
100 μM
500 μM
G
Total NAD & NADH
NAD/NADH ratio
Luminescence (RLU)
NAD+/NADH Ratio
cDMEM ΔTRP
cDMEM TRP×16
H
Aspartate
0.1 mM
0.5 mM
1 mM
5 mM
10 mM

Figure S4

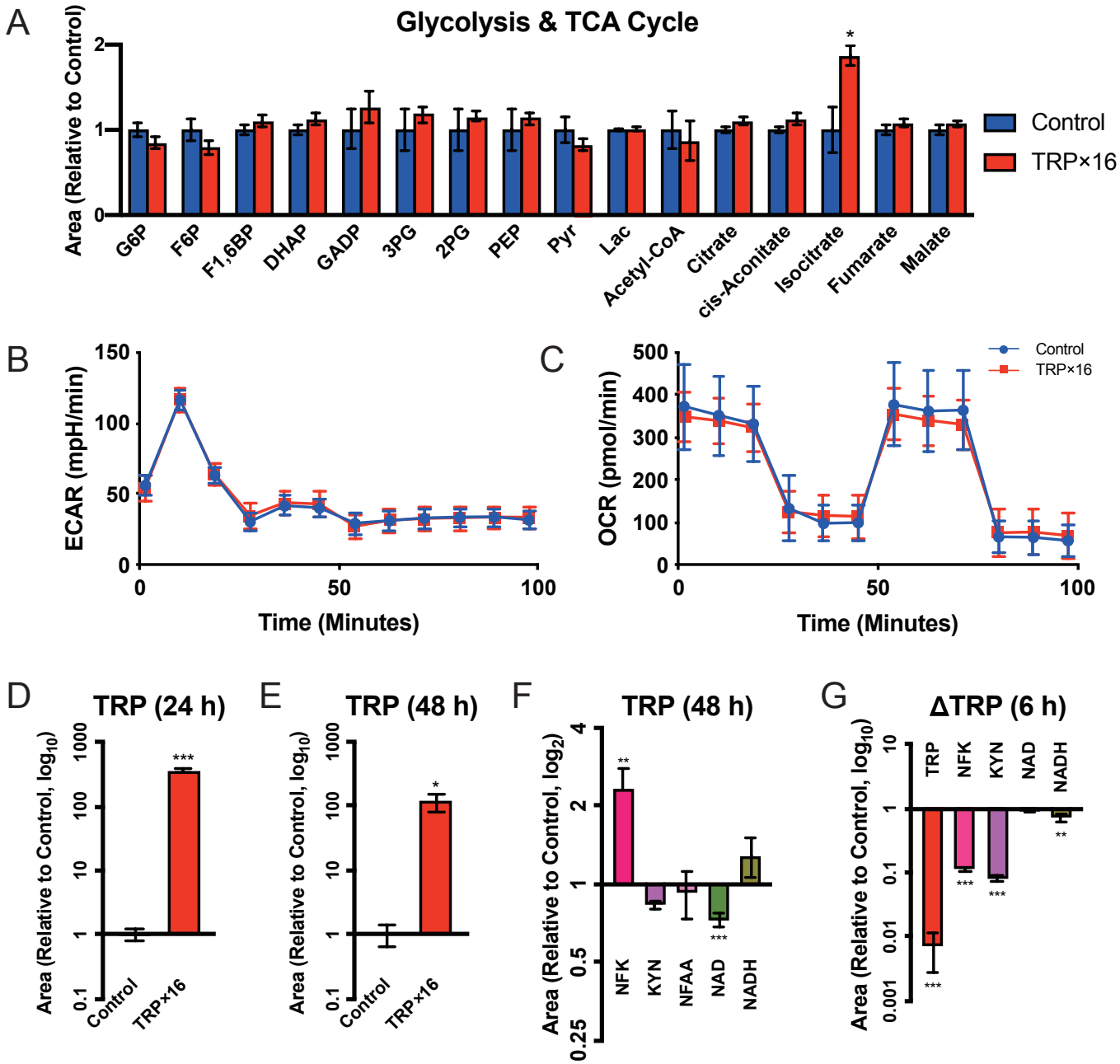
A
Glycolysis & TCA Cycle
Area (Relative to Control)
Control
TRP×16
G6P
F6P
F1,6BP
DHAP
GADP
3PG
2PG
PEP
Pyr
Lac
Acetyl-CoA
Citrate
cis-Aconitate
Isocitrate
Fumarate
Malate
B
ECAR (mpH/min)
Time (Minutes)
C
OCR (pmol/min)
Time (Minutes)
D
TRP (24 h)
E
TRP (48 h)
F
TRP (48 h)
NFK
KYN
NFAA
NAD
NADH
G
ΔTRP (6 h)
TRP
NFK
KYN
NAD
NADH

SUPPLEMENTARY FIGURE LEGENDS

Figure S1. TRP supplementation facilitates cell proliferation in another hiPSC line (Related to Figure 1).
(A) Confluence of hiPSCs (253G4) after 7 days of culture, where 16-fold of the original TRP concentration was added at 48 h after seeding, versus the control (Representative data from n = 3 independent experiments). Scale bar: 500 μm.

Figure S2. Influence of TRP supplementation on hESCs and immortalized cell lines, HeLa and HEK293T (Related to Figure 2).
(A) Cumulative growth curve of hESCs (H9) cultured in 16-fold TRP-supplemented medium compared to control medium by cell counts. Cells were adapted to respective medium for at least 1 week prior to the experiment. *P*-values were determined with a ratio paired t-test (n = 5 independent experiments).
(B) Cell confluence after 7 days of HeLa cell culture, with different folds of TRP concentration added at day 2 (n = 3 independent experiments).
(C) Cell confluence after 7 days of HEK293T cell culture, with different folds of TRP concentration added at day 2 (n = 6 replicates).
Data are represented as mean ± S.E.M; *$p < 0.05$; **$p < 0.01$.

Figure S3. TRP metabolism regulates proliferative capacity of hPSCs independent of AhR signaling or NAD *de novo* synthesis (Related to Figure 3).
(A) Cell confluence after 4 days of hiPSC (201B7) culture, with custom DMEM (cDMEM) medium, substituted at 48 h after seeding, and cell confluence after 7 days of hiPSC (201B7) culture, with StemFit maintenance medium, substituted at 24 h after seeding. TRP-replenished and TRP-depleted media were denoted as TRP and ΔTRP, respectively. *P*-values were determined by unpaired t-tests (n = 4).
(B) Representative immunoblot protein expressions of aryl hydrocarbon receptor (AhR) and indoleamine 2,3-dioxygenase (IDO) in hiPSCs (253G4), hESCs (H9), hiPSC (253G4)-cardiomyocytes (hiPSC-CMs) and human dermal fibroblasts (HDF) by western blot analysis, and the relative quantified protein expressions of AhR and IDO, in which hiPSC expression levels were normalized to 1. GAPDH was used as a loading control. *P*-values were determined with a ratio paired t-test (n = 3).
(C) Cell confluence after 5 days of hiPSC (201B7) culture, with different concentrations of StemRegenin-1 (SR-1) added at day 1 (n = 2 independent experiments).
(D) Cell confluence after 7 days of hiPSC (201B7) culture, with different concentrations

of 2,3,7,8-Tetrachlorodibenzo-p-dioxin (TCDD) added at day 2 (n = 3 independent experiments).
(E) Cell confluence after 5 days of hiPSC (201B7) culture, with different concentrations of Ro 61-8048 added at day 1 (n = 3 independent experiments).
(F) and (H) Cell confluence after 7 days of hiPSC (201B7) culture, with different concentrations of nicotinic acid mononucleotide (NAMN), or aspartate added at day 2 (n = 3 independent experiments).
(G) Luminescence quantification, indicating total amount of nicotinamide adenine dinucleotide (NAD) and NADH (left) (n = 24 replicates), and the ratio of NAD/NADH (right) (n = 12 replicates), comparing TRP-depleted and TRP-supplemented custom DMEM medium, denoted as cDMEM ΔTRP and cDMEM TRP×16, respectively.
Data are represented as mean ± S.E.M; *$p < 0.05$; **$p < 0.01$; ***$p < 0.001$.

Figure S4. Metabolic changes in hiPSCs under TRP-supplemented or depleted conditions (Related to Figure 4).
(A) Metabolome analysis of glycolysis and TCA cycle-associated metabolites comparing hiPSCs (201B7) incubated with or without TRP-supplemented medium for 24 h, as analyzed by CE-FTMS. *P*-values were determined with an unpaired t-test (n = 5 replicates).
(B) and (C) Extracellular acidification rate (ECAR), and oxygen consumption rate (OCR) of hiPSCs (201B7) with or without TRP supplementation (n = 10 replicates).
(D) and (E) Analysis of CE- FTMS showing relative concentration of TRP after exposure to TRP-supplemented medium for 24 and 48 h, respectively, where *P*-values were determined by unpaired t-tests (n = 5 replicates).
(F) Change in the normalized relative intracellular concentrations of KYN pathway metabolites after TRP exposure for 48 h as determined by CE-FTMS. *P*-values were determined with an unpaired t-test, comparing the raw results of each metabolite (n = 5 replicates).
(G) Changes in the normalized relative intracellular concentrations of KYN pathway metabolites after TRP depletion for 6 h as determined by CE-FTMS. *P*-values were determined with an unpaired t-test, comparing the raw results of each metabolite (n = 5 replicates).
Data are represented as mean ± S.E.M; *$p < 0.05$; **$p < 0.01$; ***$p < 0.001$.

TRANSPARENT METHODS

Cell Lines

The hiPSC lines (201B7 and 253G4) were provided by the Center for iPS Cell Research and Application, Kyoto University. The ESC line (H9) was provided by WiCELL, and our use complied with the Guidelines on the Distribution and Utilization of Human Embryonic Stem cells, Ministry of Education, Culture, Sports, Science and Technology, Japan. The HEK293T line, HeLa line, and HepG2 line were provided by RIKEN BioResource Research Center, the human dermal fibroblasts line was purchased from Thermo Fisher Scientific, and were maintained in DMEM (Gibco, 11885) supplemented with 10% FBS (Biowest, S1560-500) on 0.1% gelatin scaffolds. Cells were dissociated using 0.25% Trypsin/1 mM EDTA (Nacalai tesque, 35554-64) for passaging. hiPSCs (253G4)-derived cardiomyocytes were obtained and purified using previously described methods (Tohyama et al., 2017; 2016). All cell lines were grown within a humidified 5% CO_2 incubator at 37℃, and were regularly tested for Mycoplasma infection.

Maintenance of hiPSCs or hESCs

hiPSCs were routinely passaged every 7 days. After cells were washed with D-PBS (FUJIFILM Wako Pure Chemical, 045-29795), TrypLE Select (Gibco, 12563011) was applied and cells were incubated at 37°C under 5% CO_2 for 3–5 min. Dissociated single cells were collected in growth medium containing mTeSR1 (STEMCELL Technologies, 85850) with 10 μM of CultureSure Y-27632 (FUJIFILM Wako Pure Chemical, 034-24024). Following centrifugation (300 x g for 4 min), supernatant aspiration and addition of growth medium mixture, a cell count was performed with a Vi-CELL XR (Beckman Coulter), and cells were then seeded onto growth factor-reduced Matrigel (Corning, 354230) coated plates. For cumulative cell counts, 1×10^5 cells were seeded onto a 10 cm dish. Medium was changed every other day using mTeSR1 without Y-27632 unless otherwise stated (Nakagawa et al., 2014). In specified experiments, hiPSCs were maintained with modified StemFit medium, AS103C (Ajinomoto). Karyotypes of hiPSCs were analyzed by Nihon Gene Research Laboratories Inc., Sendai, Japan.

Preparation of Special Growth Media

Key reagents used were: L-alanine (Sigma, A7469), L-arginine monohydrochloride (Sigma, A6969), L-asparagine monohydrate (Sigma, A7094), L-aspartic acid (Sigma, A7219), L-cysteine hydrochloride monohydrate (Sigma-Aldrich, C6852), L-glutamic acid (Sigma, G8415), L-glutamine (Sigma, G8540), glycine (Sigma, G8790), L-histidine

monohydrochloride monohydrate (Sigma, H5659), L-isoleucine (Sigma, I7403), L-leucine (Sigma, L8912), L-lysine monohydrochloride (Sigma, L8662), L-methionine (Sigma, M5308), L-phenylalanine (Sigma, P5482), L-proline (Sigma, P5607), L-serine (Sigma, S4311), L-threonine (Sigma, T8441), L-tryptophan (L-TRP) (Sigma, T8941), L-tyrosine disodium dihydrate (Sigma, RES3156T-A7), L-valine (Sigma, V0513), Ro 61-8048 (Sigma, SML0233), AhR Antagonist II SR1 (Sigma, 182706), 2,3,7,8-tetrachlorodibenzo-p-dioxin (Supelco, 48599), nicotinic acid mononucleotide (Sigma, N7764) and N-formylkynurenine (NFK) (Toronto Research Chemicals, F700490). TRP-supplemented mTeSR1 medium was prepared through addition of L-TRP in 4-16-fold increments of the original concentration (3.46×10^{-2} mM) (Ludwig et al., 2006). Similarly, TRP-supplemented DMEM for HeLa and HEK293T cell lines was prepared by adding L-TRP incrementally based on the original concentration (7.83×10^{-2} mM). TRP-depleted custom DMEM medium was prepared through addition of 20 mM of D(+)-glucose (FUJIFILM Wako Pure Chemical, 049-31165), 2.26×10^{-1} mM of bovine albumin fraction V Solution (Gibco, 15260037), Insulin (3.44×10^{-3} mM), Transferrin (1.38×10^{-4} mM), Selenium (7.75×10^{-5} mM) Solution (Gibco, 41400045), and 0.6 mM of L-Ascorbic Acid (Sigma, A5960) into glucose- and TRP-depleted DMEM medium kindly provided by Ajinomoto; TRP-replenished or 16-fold TRP-supplemented custom DMEM medium was prepared with 3.46×10^{-2} mM or 5.54×10^{-1} mM of L-TRP respectively. TRP-depleted StemFit medium was kindly provided by Ajinomoto; TRP-replenished AS103 medium was prepared with 3.46×10^{-2} mM of L-TRP. Culture medium from the same lot was used for each experiment. Modified culture media were sterile filtered, and their volume was equalized to controls by adding DMSO (Sigma, D2650) and/or Milli-Q H_2O where necessary. For acidic or basic reagents, pH of the solutions was adjusted using hydrochloric acid solution (Sigma, H9892) or sodium hydroxide solution (Sigma, S2770), and verified by Twin pH (Horiba). Solutions were stored in the dark at 4 °C, and if an original reagent required -20 °C storage, the solution prepared was divided into aliquots to minimize thaw-freeze cycles.

Measurements of AA Consumption and Secretion of KYN and NFK

Unused mTeSR1 medium overlying on a Matrigel-coated plate was sampled, and hiPSCs (2.5×10^5) were then cultured in mTeSR1 with 10 μM of Y-27632 for 24, 48 or 72 h without medium change, and supernatant samples were stored at -80 °C until analysis. The fraction concentration of AAs as well as concentration of KYN in the consumed medium was measured with the LC-MS/MS system, as previously described (Shimbo et al., 2009; Tohyama et al., 2016). For measurement of KYN and NFK secretion, hiPSCs

(3.5×10^5) were cultured in mTeSR1 with 10 μM of Y-27632 for 2 days. Following removal of the supernatants, the cells were either left untreated or treated with TRP. Samples were collected every day and the media was changed every 48 h.

Cell Proliferation Assays

IncuCyte ZOOM (Essen Bioscience) was used for imaging assessment of cell proliferation by measuring cell confluence serially for specified periods. For hiPSCs or hESCs, 3×10^4 cells were plated in 6-well plates with the exception of assays using NFK, for which 1×10^5 cells were plated; while those including addition of inhibitors, Ro 61-8048 and SR-1, were plated at 2.5×10^5 cells; for AhR and IDO siRNAs, 2.5×10^5 cells were seeded. Alternatively, 2×10^4 HeLa cells and 1×10^4 HEK293T cells were seeded into 6-well plates. Cells were routinely incubated for 48 h in normal condition for stabilization, before transfer into medium consisting of compound to be tested, except for most of the inhibition assays mentioned above, where cells were incubated for 24 h. Cell confluence was calculated by imaging cells with whole-cell phase contrast imaging serially from the day of the initial medium change, using a lens apparatus and the following software recognition and analysis of cell confluence. For cell counts, Vi-CELL XR was used after specified periods of culture in a likewise manner.

Alkaline Phosphatase Staining

Plate wells were washed with D-PBS, and 4% paraformaldehyde fixative (Muto Pure Chemicals, 33111) was applied for 20 min before aspiration and washing with Milli-Q H_2O. A cocktail of FRV-Alkaline Solution, Sodium Nitrate Solution, Naphthol AS-BI Alkaline Solution of Leukocyte Alkaline Phosphatase Kit (Sigma, 86R), and Milli-Q H_2O was added to the well according to the manufacturer's instructions, and was shielded from light for 20–30 min prior to inspection.

Immunocytochemistry

Cells were washed once with D-PBS and fixed by adding 4% paraformaldehyde for 30-60 min. Cells were then washed twice more with D-PBS, and 0.1% Triton X was added for 1–15 min to permeabilize cells. Cells were then washed with PBS and blocked with ImmunoBlock (KAC, CTKN001) for 1 h or overnight. Following subsequent incubation with a primary antibody diluted in ImmunoBlock overnight at 4 °C, cells were washed twice with PBS, and co-incubated with a secondary antibody and 300 nM DAPI (Molecular Probes, D3571) for 2 h at room temperature in the dark. Finally, cells were washed twice with PBS and incubated in ImmunoBlock until staining was examined with

the inverted microscope Axio Observer.D1 (ZEISS) utilizing the accompanying software AxioVision (ZEISS). Primary antibodies used were: anti-OCT-3/4 (Santa Cruz, sc-5279; 1:200), anti-NANOG (ReproCELL, RCA0003P; 1:100), anti-SSEA4 (Chemicron, MAB4304; 1:200), anti-TRA-1-60 (Chemicron, MAB4360; 1:200), anti-IDO (Abcam, ab211017; 1:1000). Secondary antibodies used were: donkey anti-Mouse IgG (H+L), Alexa Fluor 488 (Molecular Probes, A-21202; 1:200), goat anti-Mouse IgM Heavy Chain Cross-Adsorbed, Alexa Fluor 488 (Molecular Probes, A-21042; 1:200), goat anti-Rabbit IgG (H+L) Cross-Adsorbed, Alexa Fluor 488 (Molecular Probes, A-11008; 1:200), and donkey anti-rabbit IgG (H+L) Highly Cross-Absorbed, Alexa Fluor 594 (Molecular Probes, A-21207).

Flow Cytometry Analysis

Dissociated single cells containing growth medium were centrifuged (300 g × 4 min) and dispensed into aliquot tubes with 100 µL of a solution containing 2% FBS in D-PBS, with 10 µL of the specific antibody added to each tube. The cells were left in the dark on ice for 30 min, and an additional 1 mL of solution was added before centrifugation (1,250 x g for 3 min). Supernatants were aspirated and after mixing of 500 µL of the added solution, cells were analyzed using a Gallios Flow Cytometer (Beckman Coulter). Antibodies used were: Anti-REA Control (S)-PE, human (Miltenyi Biotec, 130-104-612), Anti-SSEA-4-PE, human (Miltenyi Biotec, 130-100-635) and Anti-TRA-1-60-PE, human (Miltenyi Biotec, 130-100-350).

Immunoblot Analysis for Protein Expression

All procedures were performed in accordance to the manufacturer's instructions. Cell lysates were prepared by addition of a mixture of NuPAGE LDS Sample Buffer (Invitrogen, NP0007), NuPAGE Sample Reducing Agent (Invitrogen, NP0009), and Milli-Q H_2O at a ratio of 5:2:13, followed by cell scraping and serial homogenization with an ultrasonic disruptor UR-21P (TOMY). Whole protein quantification was performed with a Qubit 3.0 (Thermo Fisher). After 10 min of heating at 70 °C, a gel electrophoresis was performed with a NuPAGE 4-12% Bis-Tris Gel (Invitrogen, NP0321) in Mini Gel Tank (Life Technologies) filled with 5% NuPAGE MES SDS Running Buffer (Invitrogen, NP0002), and with a PowerEase 300W Power Supply (Invitrogen). Upon completion, separated proteins were transferred onto a membrane using a PVDF mini iBlot 2 Transfer Stack (Invitrogen, IB24002) and iBlot 2 Gel Transfer Device (Invitrogen, IB21001). The membrane was then blocked with Blocking One (Nacalai tesque, 03953) for 30 min, washed by Milli-Q H_2O for 5 min, and incubated

with a primary antibody diluted in T-BST (Takara, T9142) with rotation for 1 h. The membrane was then buffered with T-BST for 5 min (repeated 3x), inoculated with a HRP-conjugated secondary antibody (Sigma) for 30 min, buffered by TBS-T for 5 min (repeated 3x), and washed with Milli-Q H_2O for 2 min (repeated 2x) in rotation, prior to visualization by Chemi-Lumi One (Nacalai tesque, 07880) or SuperSignal West Femto Maximum Sensitivity Substrate (Thermo Fisher, 34095). Images were obtained by a luminescent image analyzer LAS-3000 (FUJIFILM) or iBright FL1000 (Thermo Fisher Scientific), and band intensities were quantified by ImageJ (NIH). Primary antibodies used were: anti-GAPDH (Ambion, AM4300; 1:4000–1:25,000), anti-IDO (Abcam, ab211017; 1:1000) and anti-AHR (Abcam, ab190797; 1:1000).

siRNA Knock Down of Gene Expression

Lipofection was carried out in accordance with the manufacturer's instructions. At the time of medium change, a lipid-siRNA complex mixture of 9 μL of Lipofectamine RNA iMAX Reagent (Invitrogen, 13778) containing 150 μL of Opti-MEM (Gibco, 31985), and 25 pmol of siRNA with 150 μL Opti-MEM, was incubated for 5 min and added to a 6-well plate for analysis. siRNAs used were: Negative Control No. 1 Silencer (Ambion, A4611), IDO1 Silencer Select (Ambion, s7425) and AHR Silencer Select (Ambion, s1198).

NAD/NADH Assay

For individual quantification of NAD and NADH content, 2×10^4 cells/well were seeded onto a white 96-well plate (Corning, 3917), under normal growth conditions with 200 μL of mTeSR1 medium, and after 24 h wells were assigned into groups, where each group underwent a medium change with 200 μL of the specified medium. The cells were then incubated overnight before the NAD/NADH-Glo Assay (Promega, G9071) was performed, as per the manufacturer's instructions. Luminescence was scanned by EnSpire (Perkin Elmer).

Metabolome Analysis

hiPSCs 201B7 were cultured under normal maintenance conditions with mTeSR1 medium for 6 days and were either untreated or treated with TRP (for a final concentration of 553 μM) for 24 or 48 h. For the depletion study, after normal maintenance conditions cells were either treated with TRP-depleted StemFit or TRP-replenished StemFit medium for 6 h. For analysis of metabolites, methanol extraction was performed according to the Human Metabolome Technologies protocol. 201B7 cells were treated with 800 μL of

methanol for 30 s, and 550 μL of Milli-Q H_2O containing internal standards (solution ID: H3304-1002, Human Metabolome Technologies, Inc., Tsuruoka, Japan) was added to the methanol extract. For analysis of medium from culture cells, 80 μL of supernatant was mixed with 20 μL of Milli-Q H_2O containing the internal standards. The extract from the cells or medium was obtained and centrifuged at 2,300 × *g* at 4 °C for 5 min, and 700 μL of the upper aqueous layer was centrifugally filtered through a Millipore 5-kDa cutoff filter at 9,100 × *g* at 4 °C for 5 h to remove proteins. The filtrate was centrifugally concentrated and re-suspended in 50 μL of Milli-Q H_2O for CE-MS analysis. Metabolome measurements were carried out through a facility at Human Metabolome Technologies Inc., Tsuruoka, Japan. CE-FTMS was carried out using an Agilent CE Capillary Electrophoresis System (Agilent Technologies, Waldbronn, Germany) equipped with a Q Exactive plus (Thermo Fisher Scientific Inc., Waltham, MA, USA), Agilent 1100 isocratic HPLC pump, Agilent G1603A CE-MS adapter kit, and Agilent G1607A CE-ESI-MS sprayer kit (Agilent Technologies, Waldbronn, Germany). The systems were controlled by Agilent G2201AA ChemStation software version B.03.01 for CE (Agilent Technologies, Waldbronn, Germany) and Xcalibur (Thermo Fisher Scientific Inc., Waltham, MA, USA). The metabolites were analyzed using a fused silica capillary (50 μm *i.d.* × 80 cm total length), with commercial electrophoresis buffer (Solution ID: H3301-1001 for cation analysis and H3302-1021 for anion analysis, Human Metabolome Technologies, Inc., Tsuruoka, Japan) as the electrolyte. The sample was injected at a pressure of 50 mbar for 10 s (approximately 10 nL) for cation analysis and 25 s (approximately 25 nL) for anion analysis. The spectrometer was scanned from *m/z* 60 to 900 for cation analysis and *m/z* 70 to 1,050 for anion analysis. Other conditions were as previously described (Sasaki et al., 2019; Soga and Heiger, 2000; Soga et al., 2003; 2002). Peaks were extracted using automatic integration software TraverseMS (Reifycs Inc., Tokyo, Japan) in order to obtain peak information including *m/z*, migration time for CE-FTMS measurement (MT), and peak area. The peaks were annotated with putative metabolites from the HMT metabolite database based on their MTs in CE and *m/z* values determined by FTMS. The tolerance range for the peak annotation was configured at ±0.5 min for MT and ±3 ppm for *m/z*. In addition, peak areas were normalized against those of the internal standards, and the resultant relative area values were further normalized by sample amount.

Measurement of ECAR and OCR

hPSCs (1.2×10^5 cells) were seeded onto Matrigel-coated XF24 cell culture microplates (Seahorse Bioscience), cultured in mTeSR1 with 10 μM Y-27632, and incubated at 37 °C.

After ensuring sufficient confluency (~90%), medium was changed to glucose- and glutamine-depleted DMEM medium (Seahorse Bioscience) supplemented with 25 mM glucose, 1 mM pyruvate, 2 mM glutamine and 0.5% Insulin-Transferrin-Selenium Solution (Gibco, 41400045), and cells were grouped according to presence or absence of L-TRP (final concentration: 1.25×10^{-1} mM for TRP-supplemented; 7.83×10^{-2} mM for control). Conditioned and unconditioned cells were further incubated in a CO_2 free environment for 4 h, and OCR and ECAR were measured using a Mito Stress Kit (Seahorse Bioscience). Cells were analyzed using a XF24 Extracellular Flux Analyzer (Seahorse Bioscience) according to manufacturer's instructions.

Statistical Analysis

All statistical analysis was carried out using Prism (GraphPad). Ratio paired t-test, or unpaired t-test was employed for comparisons. Values are presented as means ± S.E.M; $*p < 0.05$; $**p < 0.01$; $***p < 0.001$.

SUPPLEMENTAL REFERENCES

Ludwig, T.E., Levenstein, M.E., Jones, J.M., Berggren, W.T., Mitchen, E.R., Frane, J.L., Crandall, L.J., Daigh, C.A., Conard, K.R., Piekarczyk, M.S., et al. (2006). Derivation of human embryonic stem cells in defined conditions. Nat. Biotechnol. *24*, 185–187.

Nakagawa, M., Taniguchi, Y., Senda, S., Takizawa, N., Ichisaka, T., Asano, K., Morizane, A., Doi, D., Takahashi, J., Nishizawa, M., et al. (2014). A novel efficient feeder-free culture system for the derivation of human induced pluripotent stem cells. Sci Rep *4*, 3594.

Sasaki, K., Sagawa, H., Suzuki, M., Yamamoto, H., Tomita, M., Soga, T., and Ohashi, Y. (2019). Metabolomics Platform with Capillary Electrophoresis Coupled with High-Resolution Mass Spectrometry for Plasma Analysis. Anal. Chem. *91*, 1295–1301.

Shimbo, K., Oonuki, T., Yahashi, A., Hirayama, K., and Miyano, H. (2009). Precolumn derivatization reagents for high-speed analysis of amines and amino acids in biological fluid using liquid chromatography/electrospray ionization tandem mass spectrometry. Rapid Commun. Mass Spectrom. *23*, 1483–1492.

Soga, T., and Heiger, D.N. (2000). Amino acid analysis by capillary electrophoresis electrospray ionization mass spectrometry. Anal. Chem. *72*, 1236–1241.

Soga, T., Ohashi, Y., Ueno, Y., Naraoka, H., Tomita, M., and Nishioka, T. (2003). Quantitative metabolome analysis using capillary electrophoresis mass spectrometry. J. Proteome Res. *2*, 488–494.

Soga, T., Ueno, Y., Naraoka, H., Ohashi, Y., Tomita, M., and Nishioka, T. (2002). Simultaneous determination of anionic intermediates for Bacillus subtilis metabolic pathways by capillary electrophoresis electrospray ionization mass spectrometry. Anal. Chem. *74*, 2233–2239.

Tohyama, S., Fujita, J., Fujita, C., Yamaguchi, M., Kanaami, S., Ohno, R., Sakamoto, K., Kodama, M., Kurokawa, J., Kanazawa, H., et al. (2017). Efficient Large-Scale 2D Culture System for Human Induced Pluripotent Stem Cells and Differentiated Cardiomyocytes. Stem Cell Reports *9*, 1406–1414.

Tohyama, S., Fujita, J., Hishiki, T., Matsuura, T., Hattori, F., Ohno, R., Kanazawa, H., Seki, T., Nakajima, K., Kishino, Y., et al. (2016). Glutamine Oxidation Is Indispensable for Survival of Human Pluripotent Stem Cells. Cell Metab. *23*, 663–674.